PRIFYSGOL CYMRU ABERTAWE
UNIVERSITY OF WALES SWANSEA

UNIVERSITY OF WALES SWANSEA

REPORT SERIES

A study on Bautista-Manero models for worm-like micellar systems

by

J. P. Aguayo and M. F. Webster

Report # CSR 5-2006

A study on Bautista-Manero models for worm-like micellar systems

J.P. Aguayo and M.F. Webster

Institute of Non-Newtonian Fluid Mechanics/EPSRC Portfolio Partnership,

Department of Computer Science, Swansea University, SA2 8PP, United Kingdom

Introduction

This study is motivated by the need to model worm-like micellar systems that arise in typical oil-recovery situations. Such systems exhibit Maxwellian-type behaviour in small-amplitude oscillatory shear and the saturation of shear stress in steady simple shear flow. Nevertheless, according to Manero and co-workers [1], their adequate representation through suitable rheological constitutive equations remains short of that desired. Good representation of the extensional properties of such viscoelastic fluid systems is also necessity if one is to sensibly predict some important phenomena that arise in porous-media flow. Here we have firmly in mind, the prediction and understanding of enhanced pressure-drop in viscoelastic systems, which is by far and away at variance from that anticipated due to the shear viscosity of the system alone, and hence, its purely viscous equivalent system.

Colloidal and polymeric liquid systems exhibit a variety of rheological responses, some of them with direct applications in the food, oil-extraction, cosmetics and coating industries. Particularly in oil-recovery processes, there is a need for fluids capable of transforming from low viscosity, Newtonian type to highly viscoelastic gels, and returning to low viscosity liquid form. These changes can be induced at different stages of the oil-recovery procedure. Viscoelastic surfactants systems (VES), with worm-like micelles formation, fall into this category and are being increasingly used as reservoir stimulation fluids, due to their assembly and disassembly properties.

Hydraulic stimulation of oil-wells is a technique to increase well-productivity when reservoir permeability is low. Fracturing treatment using viscoelastic gels is one such technique. This consists of transmitting hydraulic pressure to the rock to provoke fractures in the formation. Such a gel also contains particles (proppant), ceramic or sand, the whole constituting a porous proppant pack. The aim is for the gel to transport the pack into place and for the proppant to keep the fractures open upon removal of fluid pressure, via gel degradation. Polymeric fluids, used as fracturing liquids, present the inconvenience that they cannot be totally degraded and their particle size is sufficient to block the pores of the fracture, limiting the hydraulic conductivity of the pack. The use of viscoelastic surfactants systems as fracturing fluids, displaying worm-like micelles, has been a relatively new innovation. Once the proppant pack, armed with these fluids, comes into contact with hydrocarbon produced by the fracture, the internal structure reverts into small spherical micelles or microemulsions. As a consequence, the viscosity and

elasticity of the fluid residues fall dramatically and they are able to easily flow from the pack. Very little pore blockage is therefore encountered, so that practically full fracture flow-back efficiency is achieved, see Boek et al. [2].

Investigating the rheological response of worm-like micelles, Bautista et al. [1] proposed a model similar in structure to the Oldroyd-B constitutive equation for the evolution of stress, coupled with the Fredrickson (kinetic) equation. Such a model accounted for construction and destruction of micelles in solution, which resulted in a constitutive system capable of reproducing shear-thinning and strain-hardening/softening phenomena. The model is reported to be in excellent agreement with experimental data from steady shear and small amplitude oscillatory measurements for the EHAC surfactant. Nevertheless, the extensional viscosity of the model gives rise to unbounded response (discontinuous structure) at finite deformation rates, and as such, presents some abnormal behaviour. Since the typical extension-rates experienced in porous-media flow can enter within this range of uncertainty, it is important to rectify this position. We begin with the specification of the original Bautista-Manero (BM) model:

Extra Stress Evolution:

$$\underline{\underline{\tau}} + \frac{\eta}{G_0}\overset{\nabla}{\underline{\underline{\tau}}} = 2\eta\left(\underline{\underline{D}} + \lambda_J \overset{\nabla}{\underline{\underline{D}}}\right), \tag{1}$$

Kinetic Equation:

$$\frac{d}{dt}\left[\eta^{-1}\right] = \frac{1}{\lambda}\left(\frac{1}{\eta_0} - \frac{1}{\eta}\right) + k\left(\frac{1}{\eta_\infty} - \frac{1}{\eta}\right)\underline{\underline{\tau}} : \underline{\underline{D}}, \tag{2}$$

construction *destruction*

where the relevant parameters represent the following quantities:

λ	Structural relaxation time
λ_J	Retardation time (related to the solvent viscosity)
k	Kinetic constant for structural breakdown
η	Viscosity
η_p , η_s	Polymeric and solvent viscosities, respectively
η_0	Viscosity at zero shear-rate
η_∞	Viscosity at very high shear-rates

Modified Bautista Manero model

In order to overcome the unbounded extensional viscosity response of the original BM-model, Boek et al. (see[3]), proposed a modified Bautista-Manero (MBM) model, where the solvent and polymeric contributions are split. In this reformulation, the coefficient k/η_∞ is treated as a single parameter. The MBM constitutive equation provides a continuous extensional viscosity response, which yields the possibility of supporting

physically realistic strain-hardening/softening properties (see equations 3-5). The reformulated system now becomes:

Viscoelastic stress evolution:

$$\underline{\underline{\tau}}_p + \frac{\eta_p}{G_0}\overset{\nabla}{\underline{\underline{\tau}}}_p = 2\eta_p \underline{\underline{D}}, \tag{3}$$

Kinetic Equation:

$$\frac{\mathrm{d}}{\mathrm{d}\,\mathrm{t}}\left(\frac{1}{\eta_\mathrm{p}}\right) = \frac{1}{\lambda}\left(\frac{1}{\eta_0} - \frac{1}{\eta_\mathrm{p}}\right) + \left(\frac{\mathrm{k}}{\eta_\infty}\right)\underline{\underline{\tau}}_\mathrm{p} : \underline{\underline{\mathrm{D}}}, \tag{4}$$

Solvent contribution:

$$\underline{\underline{\tau}}_s = 2\eta_s \underline{\underline{D}}. \tag{5}$$

In order to include this model within the local finite element/volume software library, capable of 2D/3D and transient computations, it is necessary to express the system of equations in dimensionless form. This defines group numbers of Reynolds and Weissenberg number, and the following non-dimensional parameters:

$$Re = \rho\frac{\mathrm{UL}}{\mu}, \qquad We = \frac{\mu}{\mathrm{G}_0}\frac{\mathrm{U}}{\mathrm{L}}, \qquad \beta = \frac{\eta_\mathrm{s}}{\mu},$$

$$\phi_0 = \frac{\eta_0}{\mu}, \qquad \phi = \frac{\eta_{\mathrm{p}(\mathrm{t},\underline{\mathrm{x}})}}{\mu}, \qquad \omega = \lambda\frac{\mathrm{U}}{\mathrm{L}}, \tag{6}$$

$$\xi = \left(\frac{\mathrm{k}}{\eta_\infty}\right)\eta_\mathrm{s}\frac{\mathrm{U}}{\mathrm{L}}.$$

In this manner, the MBM model may be expressed in equivalent non-dimensional form:

Momentum equation:

$$Re\left[\frac{\partial}{\partial\,\mathrm{t}}\underline{\mathrm{u}} + \underline{\mathrm{u}}\cdot\nabla\underline{\mathrm{u}}\right] = -\nabla\mathrm{p} + \nabla\cdot\underline{\underline{\tau}}_\mathrm{p} + \beta\nabla^2\underline{\mathrm{u}}, \tag{7}$$

Stress evolution:

$$\underline{\underline{\tau}}_\mathrm{p} + \mathrm{We}\,\phi\overset{\nabla}{\underline{\underline{\tau}}}_\mathrm{p} = 2\phi\underline{\underline{\mathrm{D}}}, \tag{8}$$

Kinetic equation:

$$\frac{\mathrm{d}}{\mathrm{d}\,\mathrm{t}}\left(\frac{1}{\phi}\right) = \frac{1}{\omega}\left(\frac{1}{\phi_0} - \frac{1}{\phi}\right) + \left(\frac{\xi}{\beta}\right)\underline{\underline{\tau}}_\mathrm{p} : \underline{\underline{\mathrm{D}}}. \tag{9}$$

Discussion on results

Preliminary predictions have been obtained for the MBM model in a 4:1 rounded-corner planar contraction flow, under inertialess conditions (*Re*=0), with solvent/total viscosity ratio of β=1/9 (as benchmark), and zero shear viscosity of ϕ_0=8/9. This involved two separate cases, matching peaks in extensional viscosity corresponding to instances of strong hardening and moderate hardening, respectively. The comparable data (see Figure 1 for material functions) was drawn from that exhibited by an exponential Phan-Thien/Tanner (EPTT) fluid with ε_{PTT} =0.02 (strong strain-hardening) and ε_{PTT} =0.25 (moderate hardening), with which we have past experience.

Strong Hardening *Moderate Hardening*

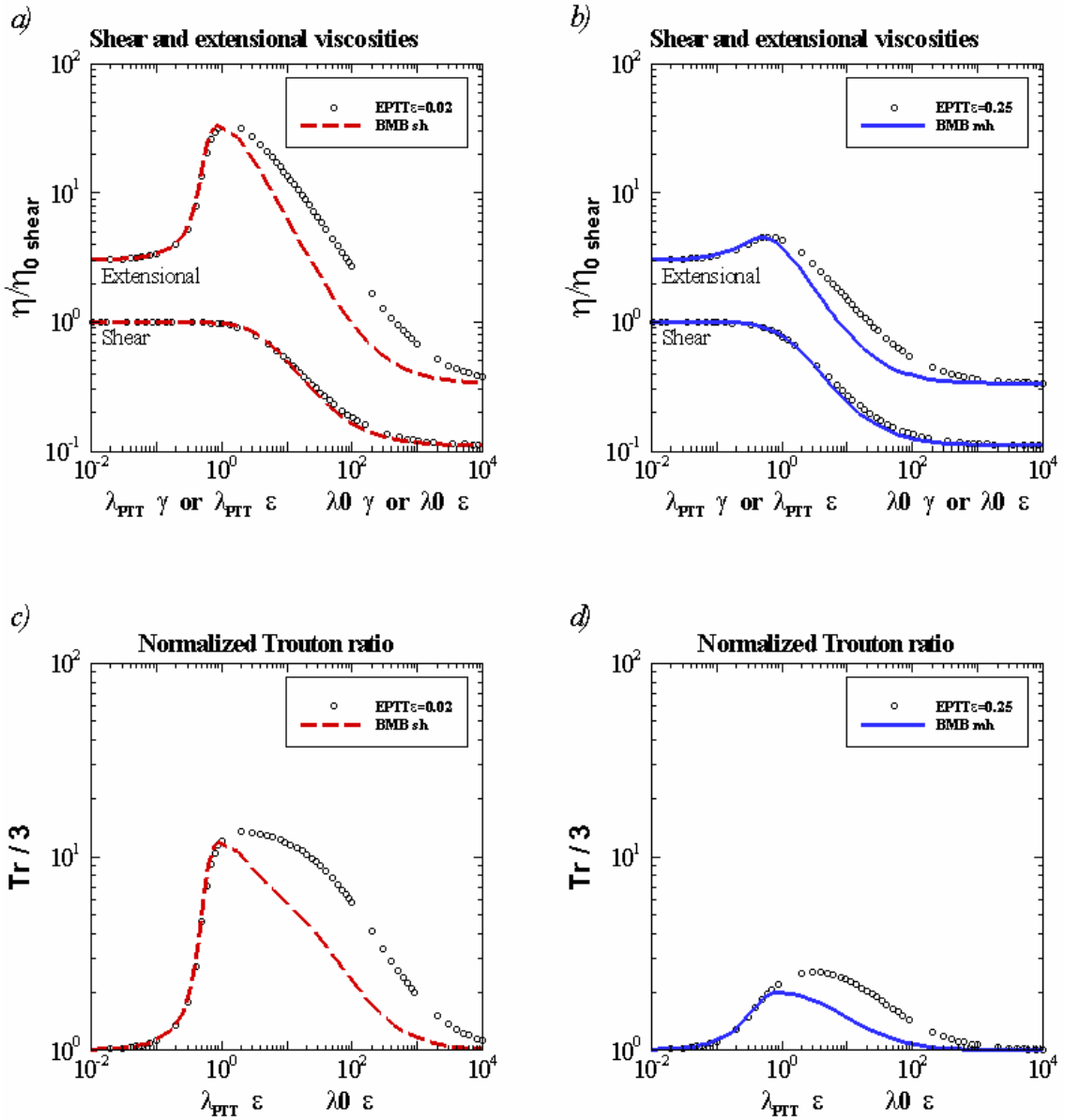

Figure 1. Shear and uniaxial extensional viscosities and Trouton ratio for both models

It can be observed that both models display the same response at low shear-rates. In shear viscosity, the agreement of fit is excellent throughout a wide range of deformation rates. Under moderate deformations rates, the MBM model softens more rapidly, reaching its plateau earlier than that for the corresponding EPTT fluid.

For the two sets of parameters chosen, vortex reduction is observed in cell-size and intensity, as displayed in Figure 2. The fluid with less degree of hardening reaches a slightly larger critical elasticity number (We_{crit}=7) when compared to that for the strongly hardening scenario (We_{crit}=5). This reduction in critical elasticity level attainable is a common feature observed when increasing strain-hardening inclusion, see Aboubacar et al. [5]. Under similar circumstances, the corresponding EPTT models provided vortex enhancement with increase of We whilst sustaining strongly-hardening properties, and only vortex reduction for the moderate hardening equivalent. This departure in response we must associate therefore with the more rapid strain-softening behaviour of the BMB-model (which is reflected also in Trouton Ratio).

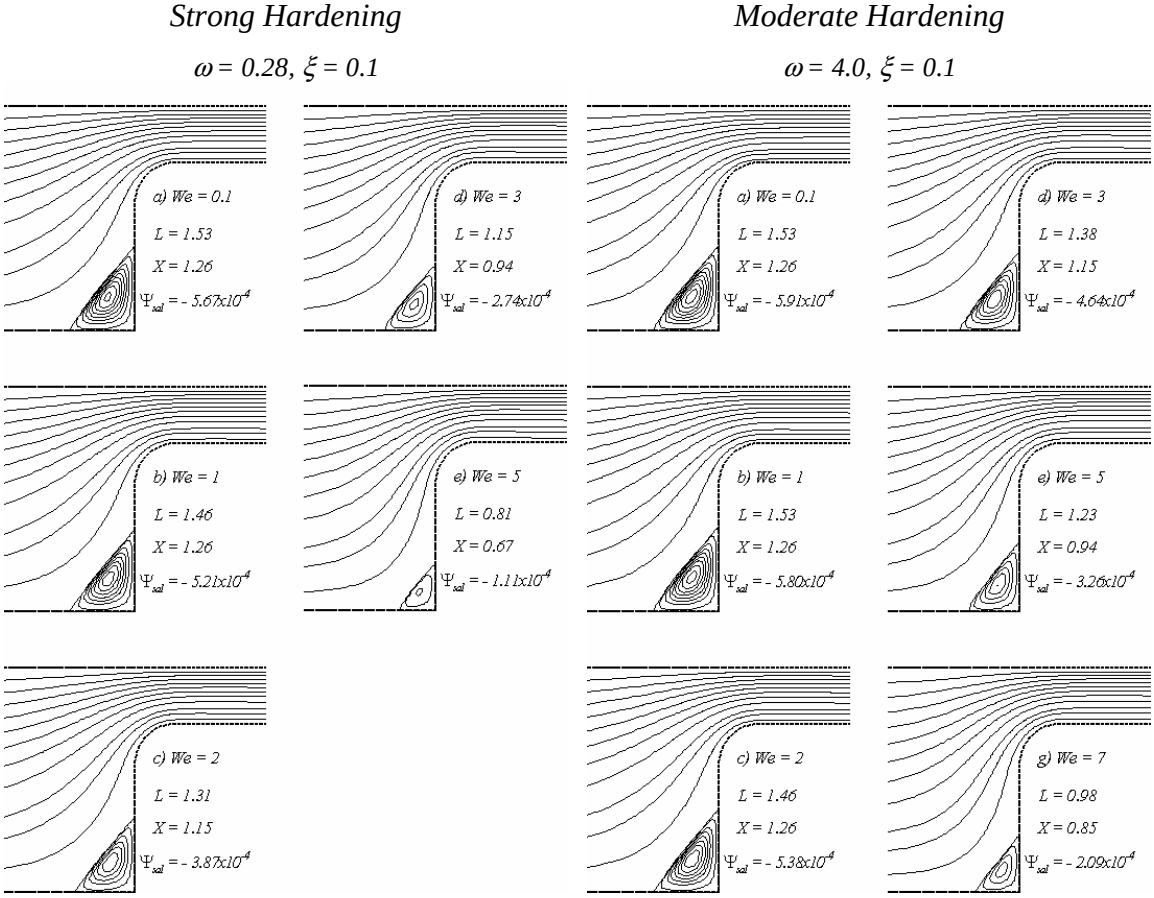

Figure 2. Streamlines for MBM model in 4:1 contraction flow

Material functions for the MBM model

In order to establish the influence of the various model parameters in viscometric flows, plots are presented varying η_0, (k/η_∞) and λ in Figures 3, 4 and 5, respectively.

Shear viscosity shifts from an almost constant level (η_0=0.01**),** approaching the Oldroyd-B response, to a case with extreme shear-thinning where the second plateau is reached at very high shear-rates. There is no visible effect on N_1 when the plot is presented in dimensionless form (Figure 3). Increasing the zero shear-rate viscosity produces an increment in the degree of strain-hardening and reduction in the level of the second plateau of η_E.

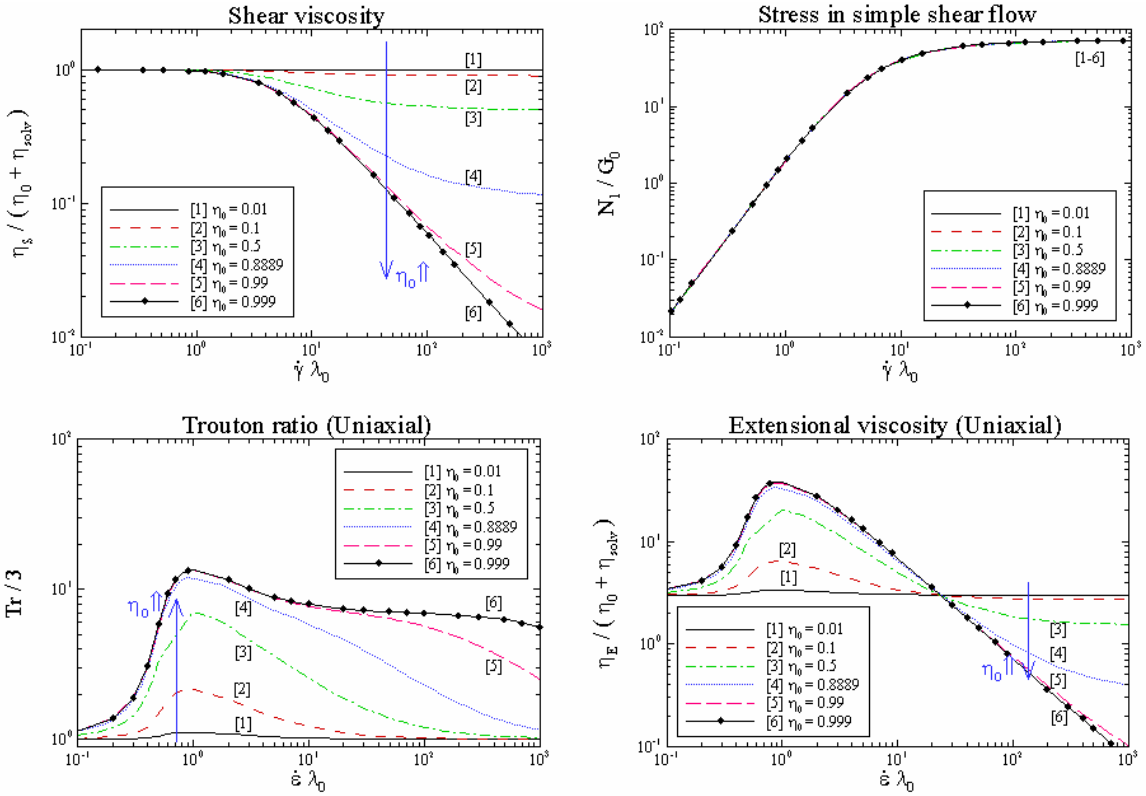

Figure 3. Shear and uniaxial response varying η_0

The influence of variation in (k/η_∞) can be gathered from Figure 4. For shear viscosity, an increase in this parameter is reflected in a decrease of the shear-rate, affecting where the thinning starts and the second plateau is reached. The levels of asymptotic plateaux are independent of (k/η_∞). From k/η_∞ =0.001 to 100, the final limiting value of the first normal stress difference decreases by more than five decades ($N_1/G_0 \approx 7\times10^4$ to 7×10^{-2}) and is attained at much lower shear-rates. A similar increment in k/η_∞ lowers the degree of strain-hardening from 3×10^3 to zero, so that for the fluid with k/η_∞ =100, η_E decreases monotonically, softening even at very low deformation rates.

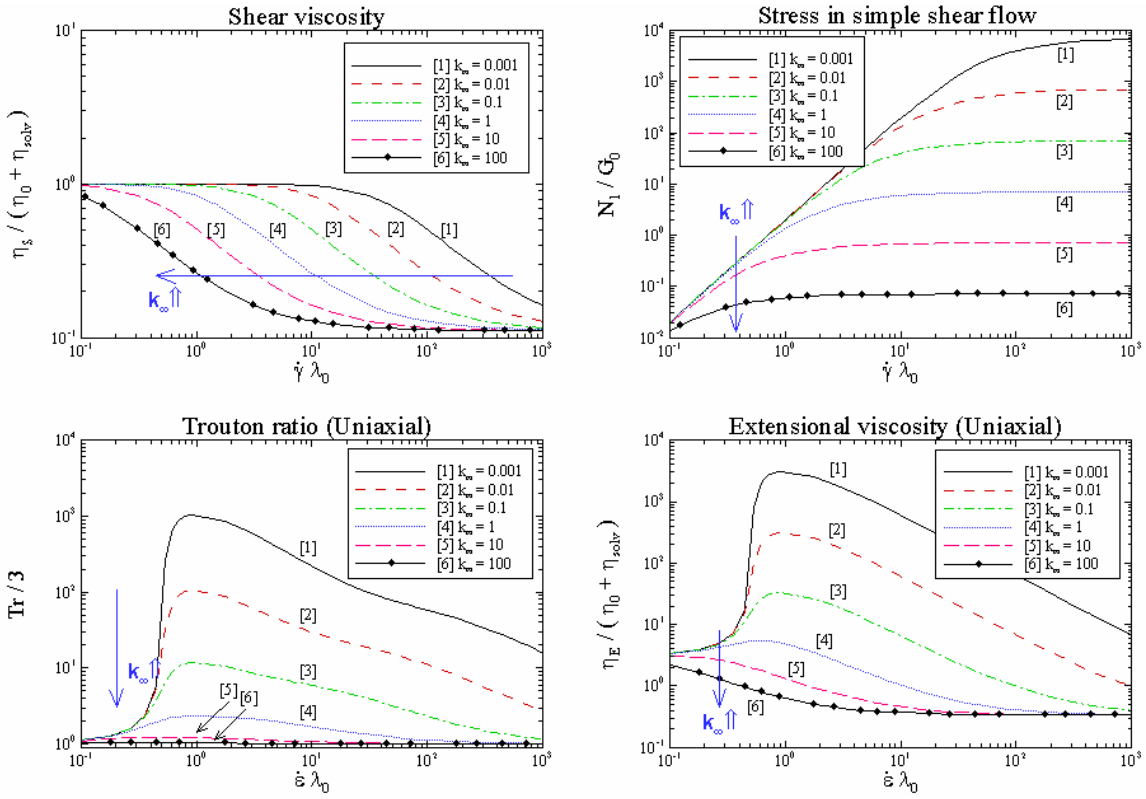

Figure 4. Shear and uniaxial response varying k/η_∞

Referring to Figure 5, the response of the model to a change in λ somewhat replicates that dealt with under k/η_∞. We can appreciate that the shear viscosity enters the thinning regime at lower deformations rates, and N_1 is decreased by about four decades when λ varies from 0.01 to 100. As above, an increase in λ produces a considerable increase in the degree of strain-hardening. Once the strain-rate transcends that associated with the peak in Trouton ratio (Tr), the second plateau in extensional viscosity is approached as strain-rates elevate further. Lower values of λ are observed to generate larger peaks in extensional viscosity and steeper softening regimes. We note that for ($\lambda \geq 10$) no strain-hardening is observed, and so no peak in extensional viscosity survives.

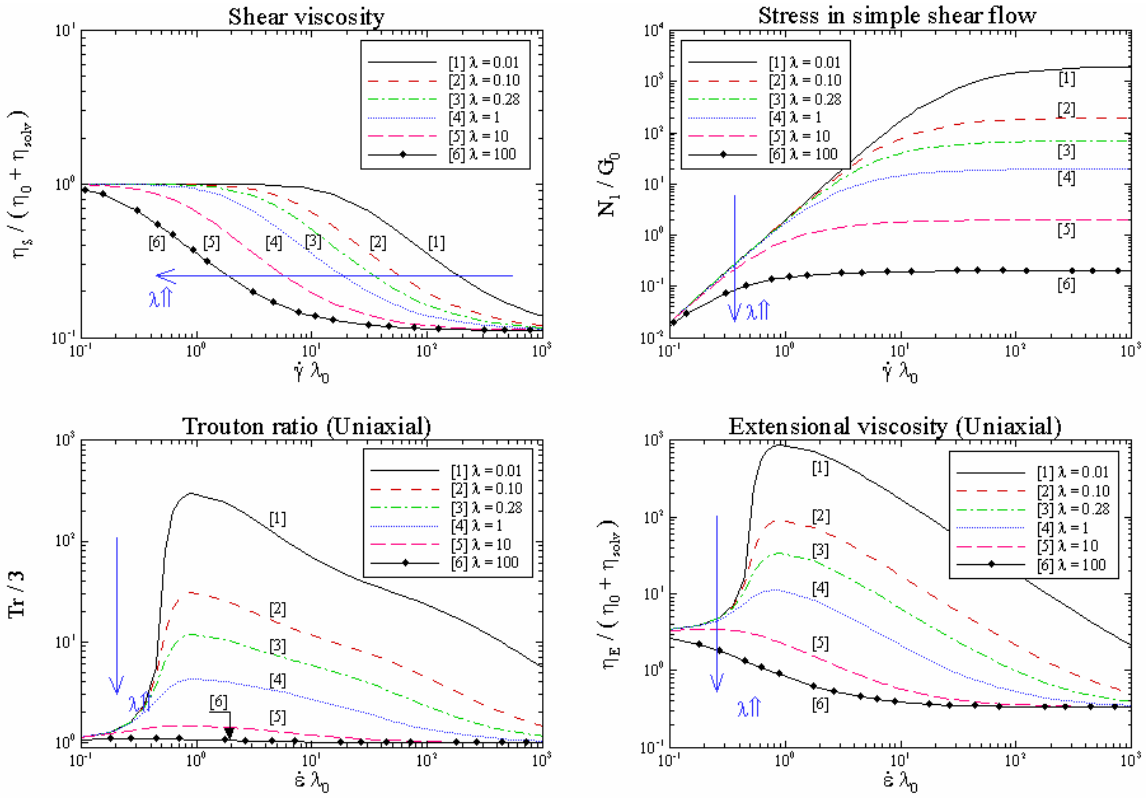

Figure 5. Shear and uniaxial response varying λ

Pressure-drop estimation in planar channels

A finite differences 1D solution has been extracted to construct steady-state pressure-drop data for the MBM fluid in a planar channel flow. The system of equations is solved for velocity and shear-rate in the cross-stream direction (dimension H), having specified the viscosity function and a characteristic pressure-drop per unit length (L) (pressure loss within the system – see below for the analytical solution). Figure 6 illustrates the division of the cross-stream domain into discrete segments and nodal points, and in general, consistency and convergence under mesh refinement has been guaranteed.

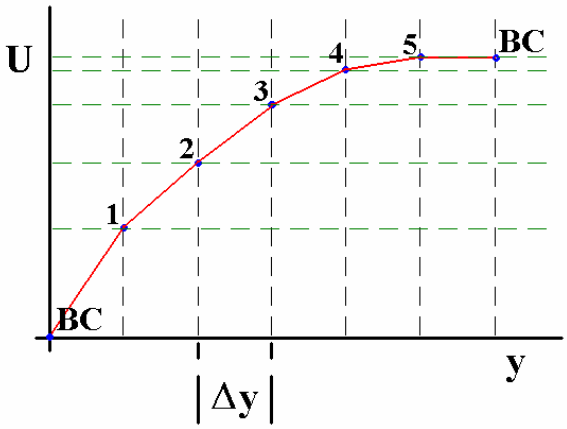

Figure 6. Schematic: cross-stream division of channel problem domain

Position in the cross-stream direction lies within $-1 \le y/\left[\frac{1}{2}H\right] \le 1$, concisely represented as $\bar{y} = y/\left[\frac{1}{2}H\right]$.

The momentum equation for the MBM model in a planar channel ($-1 \le \bar{y} \le 1$) reduces to:

$$-\tfrac{1}{2}H\frac{\Delta p}{L}\bar{y} = \left[\eta_p + \eta_s\right]\dot{\gamma} \tag{10}$$

which satisfies the mid-channel condition

$$\bar{y} = 0 \quad \Rightarrow \quad \dot{\gamma} = 0\,. \tag{11}$$

The MBM shear viscosity, η_p, is given by:

$$\eta_p = \frac{1}{2\lambda k_\infty \eta_0 \dot{\gamma}^2}\left[-1+\sqrt{1+4\lambda k_\infty \eta_0{}^2 \dot{\gamma}^2}\right] \tag{12}$$

where the parameter ($k/\eta\infty$) is represented by $k\infty$ for convenience.

Assuming a given pressure-drop per unit length to conduct the parameterisation, the solution of equation (10) at a series of $\bar{y}$-values (y_i-positions) covering the half-channel width, yields the necessary deformation rate profile. This profile may then be integrated by means of a Taylor series (Euler or similar scheme) to yield the corresponding velocity profile:

$$u_i = u_{i-1} + \Delta\bar{y}\ \dot{\gamma}_{i-1} \tag{13}$$

The boundary condition at the wall is:

$$\bar{y} = \pm 1 \quad \Rightarrow \quad u = 0 \tag{14}$$

application of which realises:

$$u_0 = 0\,. \tag{15}$$

Equation (15) is necessary as a starting point for the forward numerical integration procedure of equation (13). This procedure may be terminated at the half-length of the channel. By definition, Δy is the distance between two successive points into which the domain has been divided, see Figure 6.

Finally, it is necessary to compute the resulting flow rate (Q), which is accomplished through quadrature applied to the integral:

$$Q = 2W\,H \int_0^1 u_{(\bar{y})}\, d\bar{y} \tag{16}$$

In order to convince ourselves of algorithmic consistency and convergence upon mesh refinement with sufficient number of discrete points, Figure 7 presents the solution profile using 11, 101 and 1001 points across the domain. It is self-evident that the three solutions are in excellent agreement.

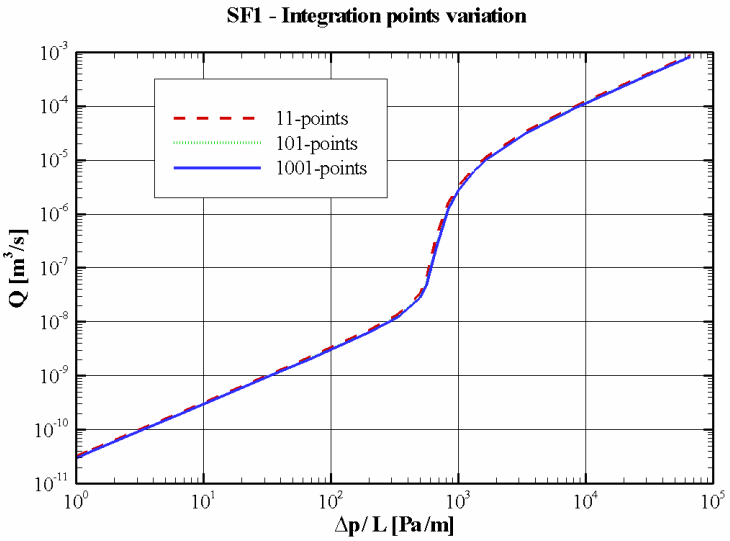

Figure 7. Solutions for different number of degrees of freedom

Once the solution has been validated, the next step to meet requirements is to produce the Q vs. Δp curves for the three channels of different gap-widths (H) covering the variation of fluid parameters supplied. Table 1 contains the corresponding data for the fluid SF1 and Figure 8 is a plot covering the flow rate vs. pressure-drop calculations.

Table 1. SF1 parameters

η_s [Pa s]	*0.0264*
η_0 [Pa s]	*11*
k/η_∞ [Pa^{-2} s^{-1}]	*0.33019*
λ [s]	*13.6284*
G_0 [Pa]	*0.44*

From Figure 8, we can gather a monotonic increasing relationship between flow rate and pressure-drop. The curves can be superimposed almost perfectly upon each other, implying that they have exactly the same trend. Nevertheless, a constant shift factor is difficult to extract as the zones where the flow rate increases faster do not start at the same level of pressure-drop. Still, one can establish a mapping as a function of H, of the start and end points of the non-linear region in pressure-drop. Linearity is upheld for low pressure-drop values (<500 Pa) and is recovered at high values (>104 Pa). For intermediate values of Δp (500<Δp<104 Pa), non-linear response is observed, so that the flow rate picks up a sudden spurt.

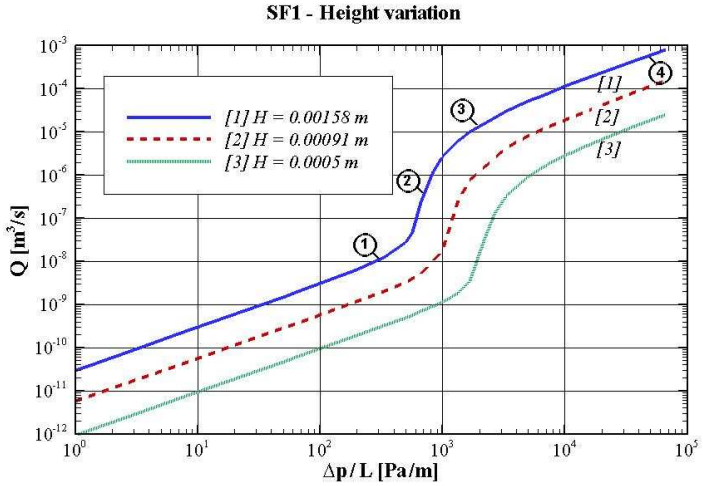

Figure 8. Q vs. Δp curves for channels of different gaps (H)

We can associate this non-linear response to the variation in shear-rate over the regions of parameters specified. The evidence for this is supplied below in Figure 9. In this figure, we can discern how the *steady* deformation rate and velocity profiles evolve when $\Delta p/L$ increases. At $\Delta p/L$=300 Pa/m (point 1), a linear shear-rate profile emerges (parabolic velocity distribution). Upon increase to $\Delta p/L$=700 Pa/m (point 2), both shear-rate and velocity profiles depart from the earlier Newtonian-like pattern; the fluid near the wall is exposed to significant variation in shear-rate, in stark opposition to the conditions approaching the centreline, where shear-rates and their variation are low. Note correspondingly, that the velocity profile is practically flat in the low shear-rate centreline

zone. It is precisely in this zone where the flow rate increases more rapidly with respect to incrementation in pressure-drop. Proceeding further to the next elevation station of $\Delta p/L$=2000 Pa/m (point 3), the Q vs. Δp curve recovers its linear relationship, so that the shear-rate profile and flow rate reform the linear and parabolic trend, respectively. We are careful to point out that, it is only when the significantly larger level of $\Delta p/L$=50000 Pa/m (point 4) is reached that such trends are effectively fully recovered. The square of the Pearson coefficient (r) through all $\dot{\gamma}$-data points (linear regression) is a measure of proximity to linearity, an r-value of unity providing a constant slope relationship. To estimate the recovery of the linear (Newtonian) $\dot{\gamma}$-profile in cases 3 and 4, we have r=0.97 for point 3 ($\Delta p/L$=2000 Pa/m), and for point 4 (($\Delta p/L$=50000 Pa/m), the r-value lies within the interval [0.99,1]. The point 4 r-value clearly exhibits a closer position to a constant slope-line than that for point 3.

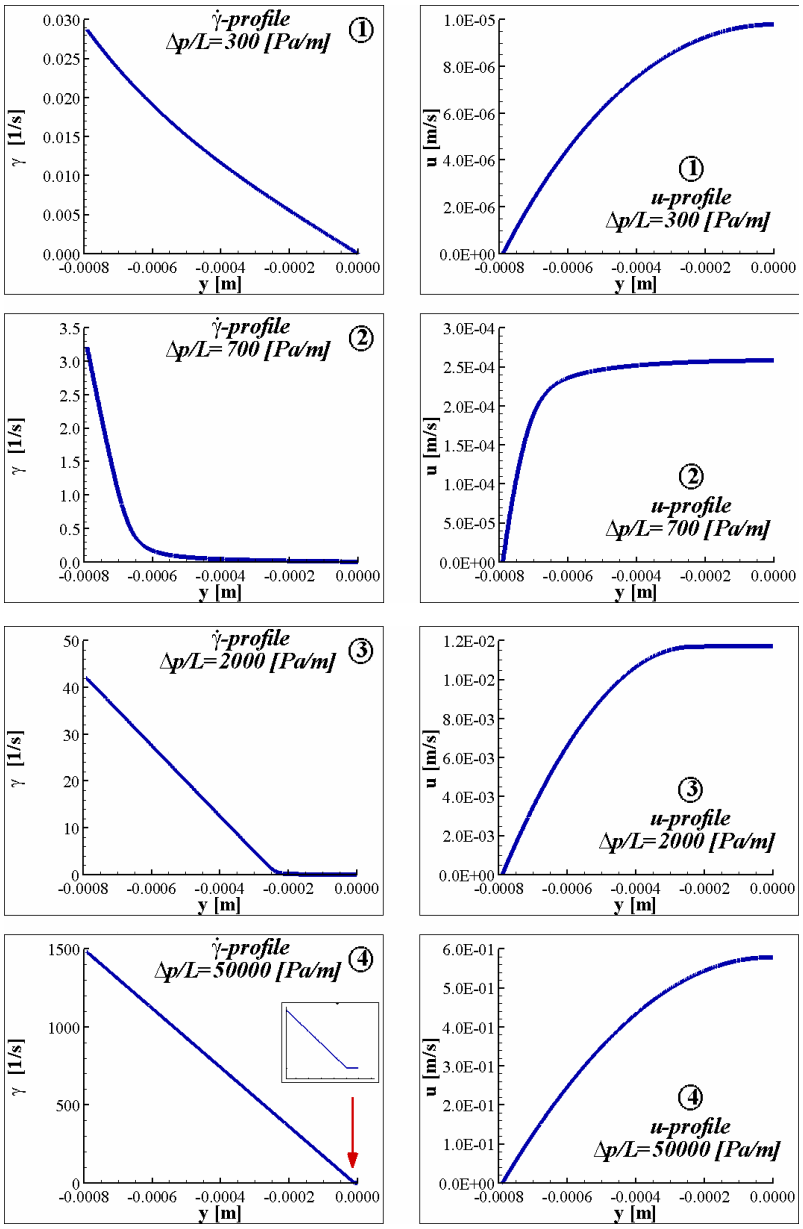

Figure 9. Evolution of deformation rate and velocity profile as Δp increases

An analytical solution

We have been able to cross-check our numerical computation above for the MBM model in planar channels by appealing to a direct procedure, and thereby, extracting an analytic solution to the problem in hand. In order to accomplish this, we appeal to an analysis for a related class of shear-thinning fluids (Oldroyd-4 constant) and shear flow in pipes performed by Walters [6]. The procedure consists in a change of variables that provides the velocity as a function of shear-rate alone.

From equation (10) (balance of forces), we can express the cross-stream y-position as a function of the deformation rate:

$$\mathrm{y} = \theta_{(\dot\gamma)} = -\left[\eta_\mathrm{p} + \eta_\mathrm{s}\right]\frac{1}{\left(\frac{\Delta \mathrm{p}}{\mathrm{L}}\right)}\dot\gamma . \tag{17}$$

Following the chain rule of differentiation, function θ satisfies:

$$\frac{1}{\dot\gamma} = \frac{\mathrm{d\,y}}{\mathrm{d\,u}} = \frac{\mathrm{d}\,\theta}{\mathrm{d}\,\dot\gamma}\frac{\mathrm{d}\,\dot\gamma}{\mathrm{d\,u}} . \tag{18}$$

Upon integrating this relationship we are able to extract the velocity as:

$$\mathrm{u} = \int \dot\gamma \frac{\mathrm{d}\,\theta}{\mathrm{d}\,\dot\gamma}\mathrm{d}\,\dot\gamma + \mathrm{C} . \tag{19}$$

With the knowledge of η_p of equation (12), the velocity, as a function of the shear-rate, is given analytically by the derived equation (20):

$$\mathrm{u}_{(\dot\gamma)} = \frac{\eta_\mathrm{s}}{2\left(\frac{\Delta \mathrm{p}}{\mathrm{L}}\right)}\left[\dot\gamma_\mathrm{x}{}^2 - \dot\gamma^2\right] + \frac{1}{2\,\mathrm{k}_\infty\,\eta_0\,\lambda\left(\frac{\Delta \mathrm{p}}{\mathrm{L}}\right)}\mathrm{Ln}\left[\frac{1+\sqrt{1+4\,\mathrm{k}_\infty\,\eta_0{}^2\,\lambda\,\dot\gamma_\mathrm{x}{}^2}}{1+\sqrt{1+4\,\mathrm{k}_\infty\,\eta_0{}^2\,\lambda\,\dot\gamma^2}}\right], \tag{20}$$

where $\dot\gamma_\mathrm{x}$ is the solution of the boundary equation at the wall ($\overline{y} = \pm 1$).

Knowing η_p, an expansion of equation (17) results in a cubic polynomial for $\dot\gamma$ as a function of $\overline{y}$, of the form,

$$\dot\gamma^3 + \mathrm{a}_1\dot\gamma^2 + \mathrm{a}_2\dot\gamma + \mathrm{a}_3 = 0 . \tag{22}$$

The respective coefficients are given by:

$$\begin{aligned} a_1 &= \frac{H}{\eta_s}\frac{\Delta p}{L}\overline{y}\,, \\ a_2 &= \frac{-\left(\eta_0+\eta_s\right) + \frac{1}{4}H^2 k_\infty \left[\frac{\Delta p}{L}\right]^2 \eta_0\,\lambda\,\overline{y}^2}{k_\infty\,\eta_0\eta_s{}^2\,\lambda}\,, \\ a_3 &= -\frac{\frac{1}{2}H\overline{y}}{k_\infty\,\eta_0\eta_s{}^2\,\lambda}\left[\frac{\Delta p}{L}\right], \end{aligned} \tag{23}$$

where we seek the real root (numerically or analytically) at any particular *y*-position across the channel. In the present instance, we have extracted the real root analytically, using the method of Cardano [7]:

$$a)\qquad \dot{\gamma}_{\text{root}\,1} = \text{Sc} + \text{Tc} - \frac{1}{3}\text{a}_1,$$

$$b)\qquad \dot{\gamma}_{\text{root}\,2} = -\frac{1}{2}(\text{Sc}+\text{Tc}) - \frac{1}{3}\text{a}_1 + \frac{1}{2}i\sqrt{3}(\text{Sc}-\text{Tc}), \tag{24}$$

$$c)\qquad \dot{\gamma}_{\text{root}\,3} = -\frac{1}{2}(\text{Sc}+\text{Tc}) - \frac{1}{3}\text{a}_1 - \frac{1}{2}i\sqrt{3}(\text{Sc}-\text{Tc}).$$

The quantities, {*Sc*, *Tc*}, necessary to evaluate these sets of solutions (roots) are defined through additional derived quantities {*Dc, Rc, Qc*}:

$$\text{Qc} = \frac{3\text{a}_2 - \text{a}_1^{\,2}}{9}, \qquad \text{Rc} = \frac{9\text{a}_1\text{a}_2 - 27\text{a}_3 - 2\text{a}_1^{\,3}}{54},$$

$$\text{Dc} = \text{Qc}^3 + \text{Rc}^2, \qquad \text{Sc} = \sqrt[3]{\text{Rc} + \sqrt{\text{Dc}}}, \tag{25}$$

$$\text{Tc} = \sqrt[3]{\text{Rc} - \sqrt{\text{Dc}}}\,.$$

The discriminant, *Dc*, reveals the nature of solutions. For the case where *Dc*<0, all three solutions are real and the following formula may be used to simplify the computation:

$$a)\qquad \dot{\gamma}_{\text{root}\,1} = 2\sqrt{-\text{Qc}}\,cos\left[\tfrac{1}{3}\varphi\right] - \frac{1}{3}\text{a}_1,$$

$$b)\qquad \dot{\gamma}_{\text{root}\,2} = 2\sqrt{-\text{Qc}}\,cos\left[\frac{\varphi + 2\pi}{3}\right] - \frac{1}{3}\text{a}_1, \tag{26}$$

$$c)\qquad \dot{\gamma}_{\text{root}\,3} = 2\sqrt{-\text{Qc}}\,cos\left[\frac{\varphi + 4\pi}{3}\right] - \frac{1}{3}\text{a}_1,$$

appealing to

$$\varphi = cos^{-1}\left[\frac{\text{Rc}}{\sqrt{-\text{Qc}^3}}\right]. \tag{27}$$

Armed with these definitions, it is the third solution root ($\dot{\gamma}_{\text{root}\,3}$), given by equations 24*c*) or 26*c*), that is equivalent to the numerical solution extracted via the proposed finite difference approximation. The deformation rate at the wall ($\dot{\gamma}_x$, required by equation 20) is:

$$a)\quad \dot{\gamma}_x = \dot{\gamma}_{root3} \quad at\ \ \bar{y} = -1, \qquad b)\quad \dot{\gamma}_x = -\dot{\gamma}_{root3} \quad at\ \ \bar{y} = 1. \tag{28}$$

For a physical solution, that smoothly varies from $\overline{y} = -1$ to the centreline ($\overline{y} = 0$), the appropriate maximum shear rate is given by equation 28*a*).

Similar procedures may be applied to many other common model viscosity functions (e.g. PTT and pom-pom), that possess a solvent viscosity component and are (or can be expressed) essentially of a polynomial form in shear-rate of integral power not greater than two (for cubics) and three for quartics. This is valid for stress evolution equations as Oldroyd-type (see eq. 3) where just first order terms of $\underline{\underline{D}}$ appear. If the constitutive model requires second order terms of $\underline{\underline{D}}$, numerical solutions may be required for the equivalent to equation 22, as quintics may appear. Third order terms are not anticipated in the constitutive equation due to the *representation theorem* (see [8]) for tensors (*Cayley-Hamilton theorem*), which indicates that terms functionally related to $\underline{\underline{D}}^3$, or higher, collapse to a function of $\underline{\underline{D}}^2$, $\underline{\underline{D}}$ and its invariants.

Pressure distributions

As the geometry does not present any constriction or change in direction for the flow, the steady pressure-drop is constant along the length of the channel, this results in a linear decay in pressure from inlet to exit. Figure 10 reflects this state of decay for two cases: the first is for a flow rate of $\approx 5 \times 10^{-6}$ m^3/s, and the second is for $\approx 5 \times 10^{-10}$ m^3/s. As anticipated, for channels with smaller heights (*H*), larger values of pressure are required to drive the flow at the same level of flow rate.

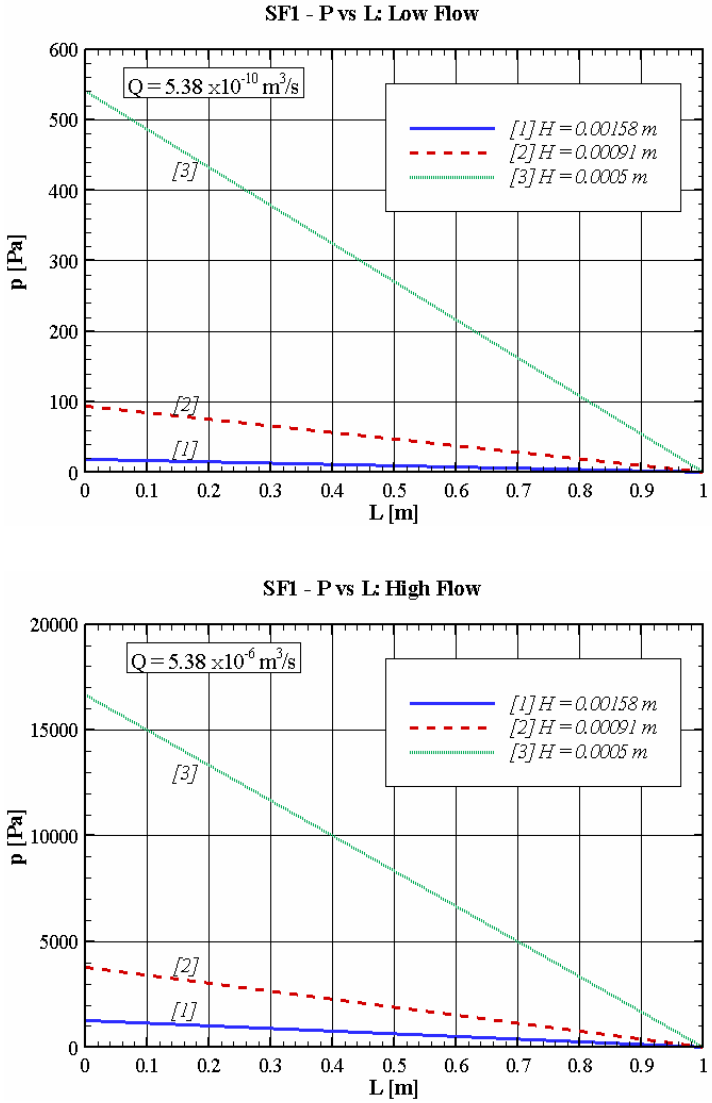

Figure 10. Pressure vs. length curves at fixed flow rate

Transient solutions

Starting from rest, we have obtained evolution field states through time by imposing a transient Oldroyd-B solution in a channel [9], at the inlet boundary (flow rate Q controlled temporal build-up). For this dynamical situation, the chosen fluid is SF2 (see Table 2) and the flow rate is 1.6×10^{-9} m^3/s.

Table 2. SF2 parameters

η_s [Pa s]	*0.0105*
η_0 [Pa s]	*2.1*
k/η_∞ [Pa^{-2} s^{-1}]	*0.6*
λ [s]	*5.0*
G_0 [Pa]	*0.525*

Pressure drop, velocity (centreline) and stress (boundary wall) are presented in non-dimensional terms in Figure 11. Pressure-drop response exhibits oscillations and is seen to reach its steady-state value faster than in velocity and stress. All evolution profiles display an overshoot. In velocity and stress, a minor undershoot is also observed before a steady-state is established.

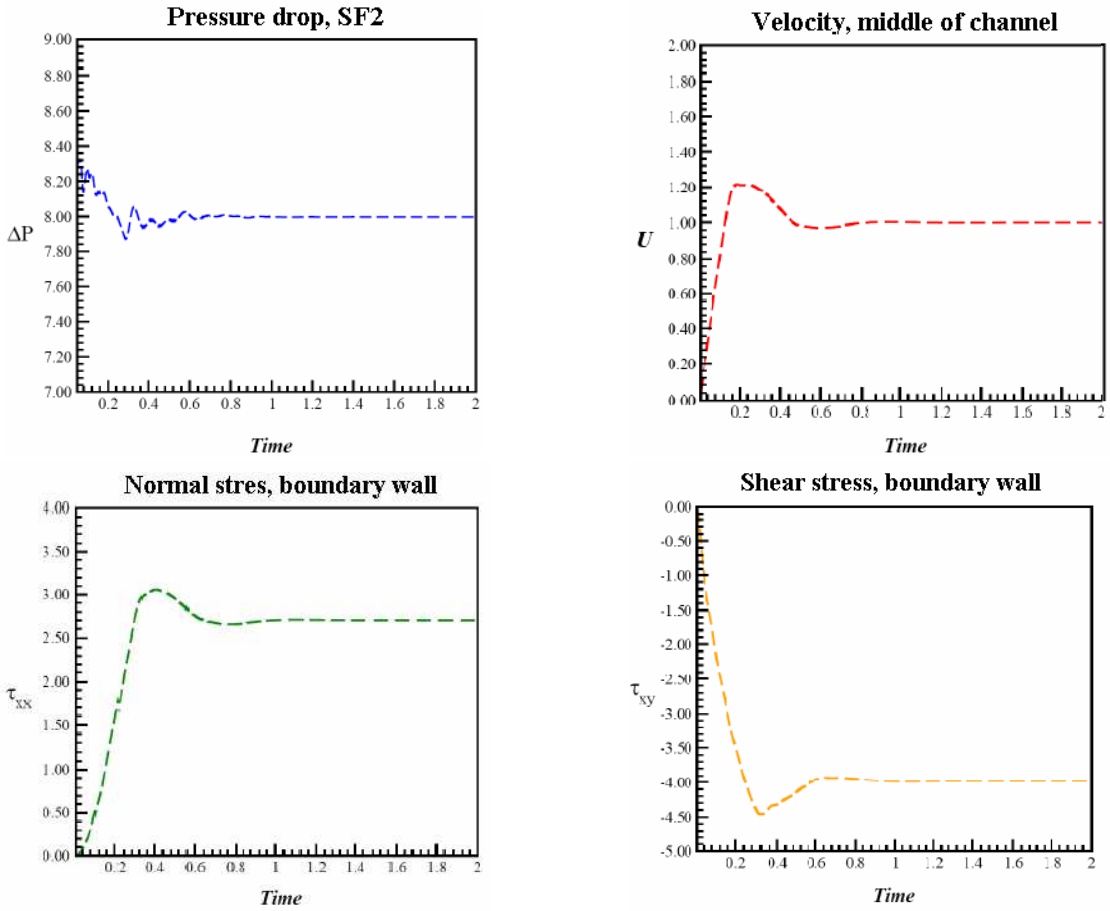

Figure 11. Transient results for the channel flow

A desirable next step would be to compute transient solutions for such fluids within a complex contraction-expansion setting, either via a flow rate controlled or a constant-force (Δp-fixed) form.

Concluding remarks

Adequate representation of worm-like micellar systems was proposed via the original Bautista-Manero (BM) model. Nevertheless, this model was found to exhibit unphysical extensional viscosity response. A modified model (MBM) was then introduced by Boek et. al., which rendered it possible to model uniaxial flow successfully.

Material functions for this new MBM version have been fitted to match two different configurations of the exponential version of the Phan-Thien/Tanner model. In contrast to the situation for pom-pom models, both extensional and shear peak viscosities can be approximated to PTT with one set of parameters alone for each different level of hardening scenario. In rheometrical flows, a variation in k/η_∞ and λ produces almost an identical response in both viscosity and stress.

Following the procedure proposed by Walters, an analytical solution $\{u,\ \dot{\gamma}\}(\bar{y})$ has been derived for the MBM model in poiseuille channel flow. The method consists in a change of variable, leaving the cross-stream position ($\bar{y}$) as a function of shear rate ($\dot{\gamma}$) and producing an integral that gives the velocity (u) in terms of the shear rate and its value at the wall. To obtain the deformation rate at the wall, the roots of a cubic polynomial must be extracted. Finally, and for confirmation of validity, the analytical solution is in excellent agreement with the results derived via a finite difference approximation.

Two linear trends for (Q vs. Δp)-variation have been detected in the corresponding solutions. These trends occur at low and high pressure-drops. There is a region where the flow rate increases faster. The behaviour in this region has been recognized to be a result of the prevailing strong shear-thinning displayed by all such fluids studied here. As such corresponding $\dot{\gamma}$-profiles display a significant departure from the linear-form anticipated over regions of nearly constant shear viscosity. Transient solutions for channel flow have also been probed, revealing their characteristic form.

References

1.- O. Manero, F. Bautista, J.F.A. Soltero, J.E. Puig. Dynamics of worm-like micelles: the Cox-Merz rule. *J. Non-Newtonian Fluid Mech. 106 (2002) 1-15*.

2.- E. S. Boek, A. Jusufi, G. C. Maitland. Molecular design of responsive fluids: molecular dynamics studies of viscoelastic surfactant solutions. J.

3.- E.S. Boek, J. T. Padding, V.J. Anderson, P.M.J. Tardy, J.P. Crawshaw, J.R.A. Pearson. Constitutive equations for extensional flow of wormlike micelles: stability analysis of the Bautista-Manero model. *J. Non-Newtonian Fluid Mech. 126 (2005) 39-46*.

4.- R.B. Bird, W.E. Stewart, E.N. Lightfoot. *Transport Phenomena*. 2nd Ed. Wiley.

5.- M. Aboubacar, H. Matallah, M.F. Webster. Highly elastic solutions for Oldroyd-B and Phan-Thien/Tanner fluids with a finite volume/element method: planar contraction flows. *J. Non-Newtonian Fluid Mech. 103 (2002) 65-103*.

6.- K. Walters. A Note on the Rectilinear Flow of Elastico-Viscous Liquids through Straight Pipes of Circular Cross-Section. *Archive for Rational Mechanics and Analysis. Vol. 9, 5, (1962) 411-414.*

7.- M. Spiegel, A. Abellanas Rapun. Fórmulas y Tablas de Matemática Aplicada. McGraw-Hill, 1992

8.- R. G. Larson, Constitutive Equations for Polymer melts and Solutions. Butterworths 1988.

9.- N.D. Waters, M.J. King, Unsteady flow of an elastico-viscous liquid, *Rheol. Acta 9 (1970) 345–355.*

Appendix: Flow rate – Pressure drop (Q vs. $\Delta P/L$) curves

MBM model parameters for all selected fluids {SFi : i=1,10} are provided in Table 3, with below, a comparable series of (Q vs. $\Delta P/L$)-plots, for each fluid in a planar channel at three different heights (H). In all configurations, the flow rate is calculated using a unit depth channel.

Table 3. Parameters for selected fluids

	η_0 [Pa s]	k/η_∞ [Pa^{-2} s^{-1}]	η_s [Pa s]	G_0 [Pa]	λ [s]
SF1	11	0.33019	0.0264	0.44	13.6284
SF2	2.1	0.6	0.0105	0.525	5
SF3	260	0.00794	0.1733	2.17	37.8
SF4	29	0.02154	0.145	2.42	7.89
SF5	300	0.00028	0.05	5	288
SF6	450	0.00093	0.06429	6.43	53.9
SF7	58	0.00292	0.05156	6.44	6.84
SF8	550	0.00108	0.066	11	27.8
SF9	85	0.00108	0.04857	12.1	12.1
SF10	1000	0.00014	0.282	47	25.8

One may gather from this (Q vs. $\Delta P/L$)-data that initial Q-values (corresponding to low pressure drops) seem to depend on the particular η_0-setting, being lower for larger viscosity values. See, for example, that SF10 presents the lowest flow rate and SF2 the highest. Additionally, we can observe that the first and second linear regimes provide slopes of unit-value.

SF1 - Height variation

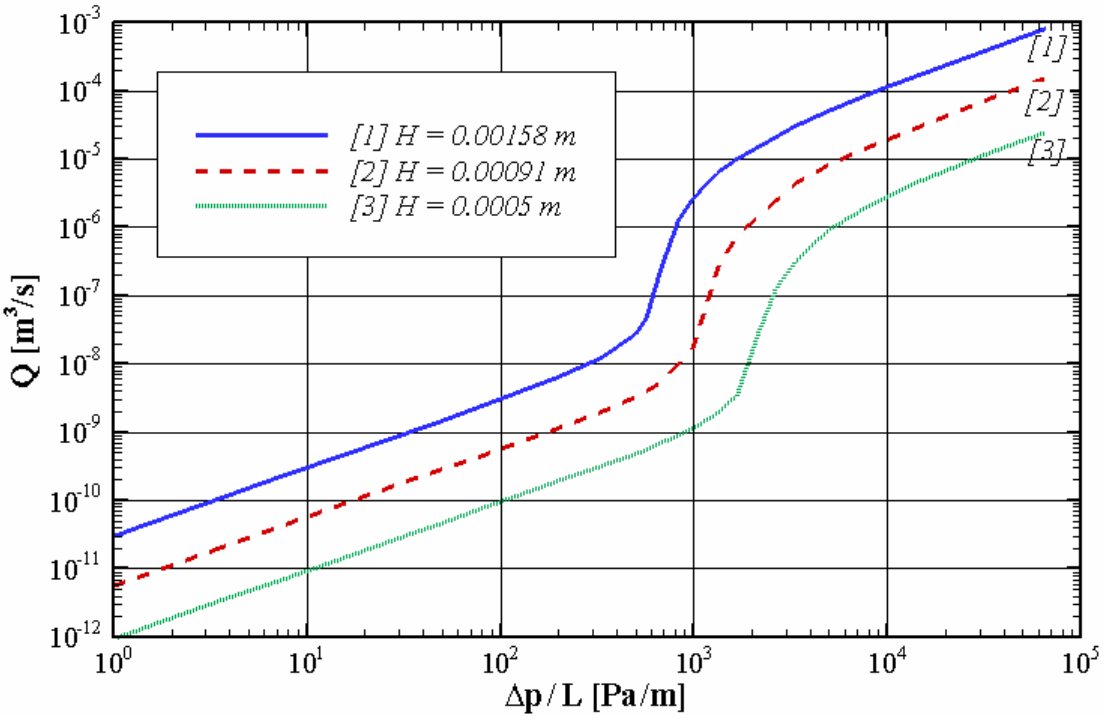

SF2 - Height variation

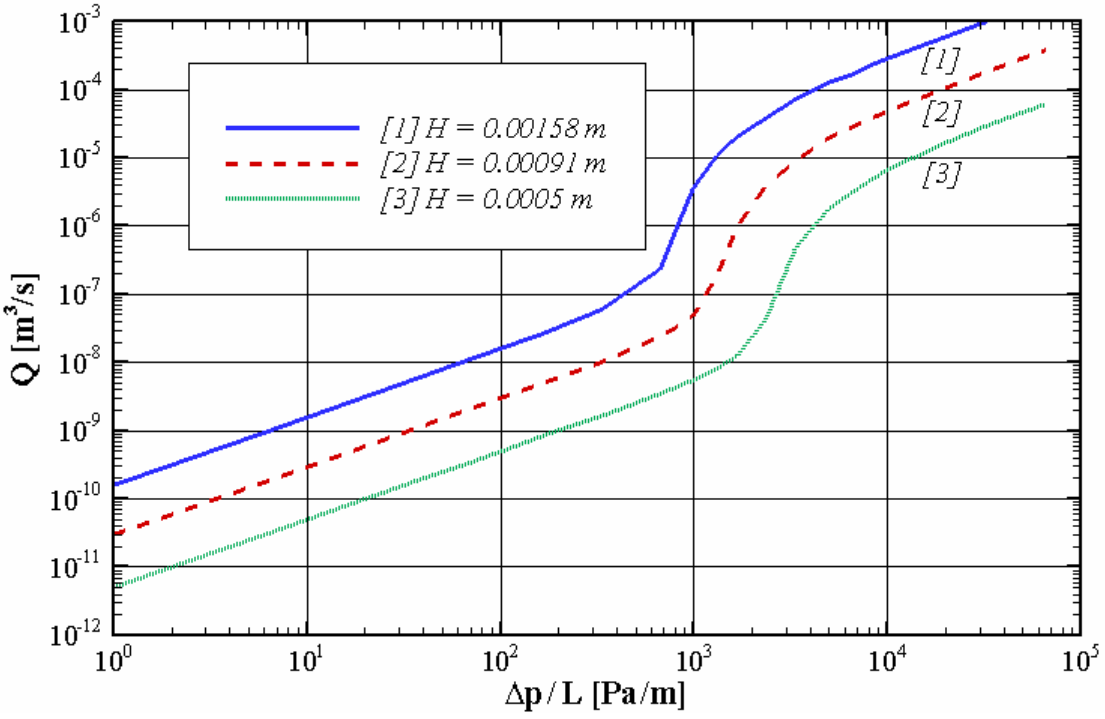

SF3 - Height variation

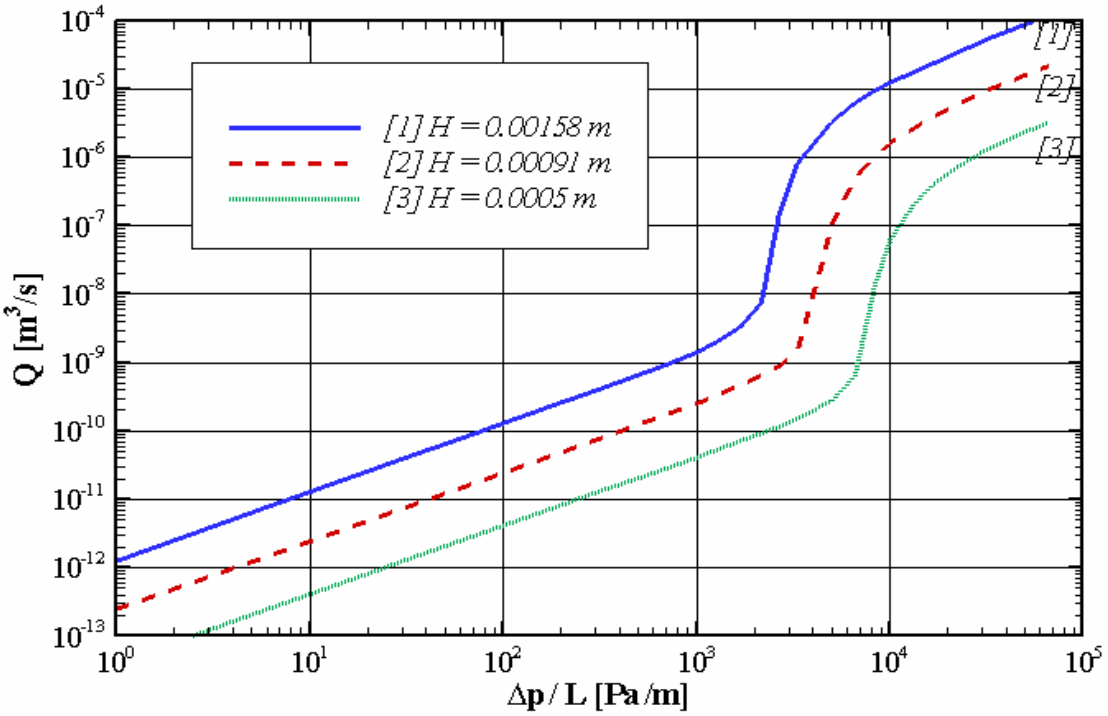

SF4 - Height variation

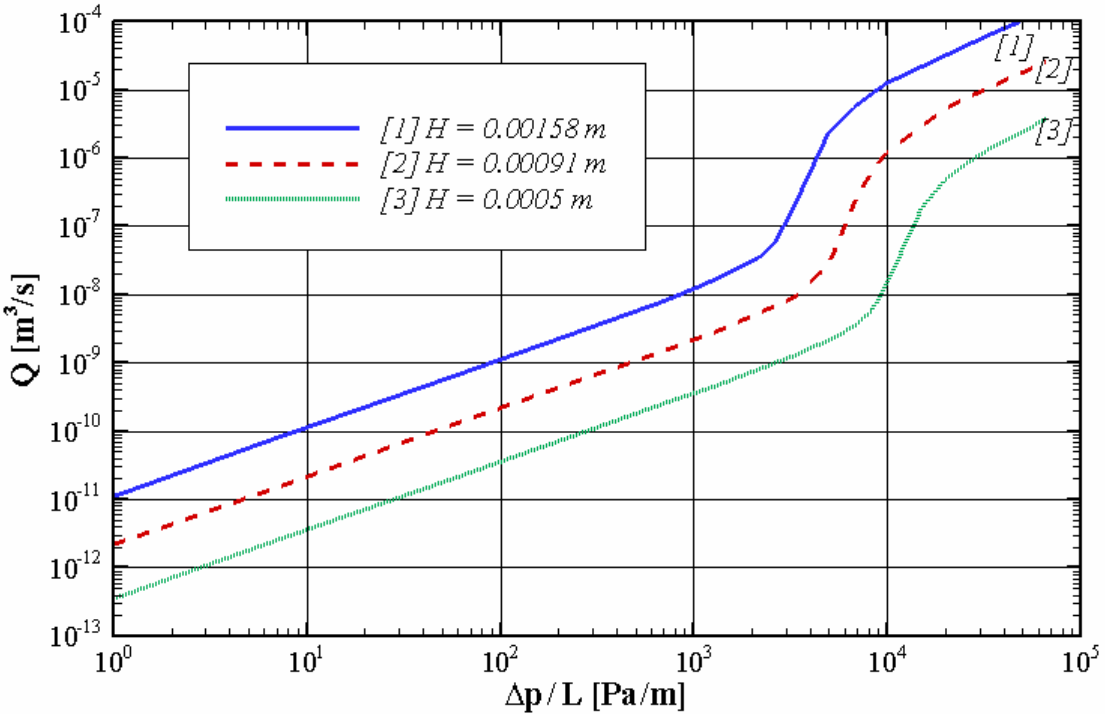

SF5 - Height variation

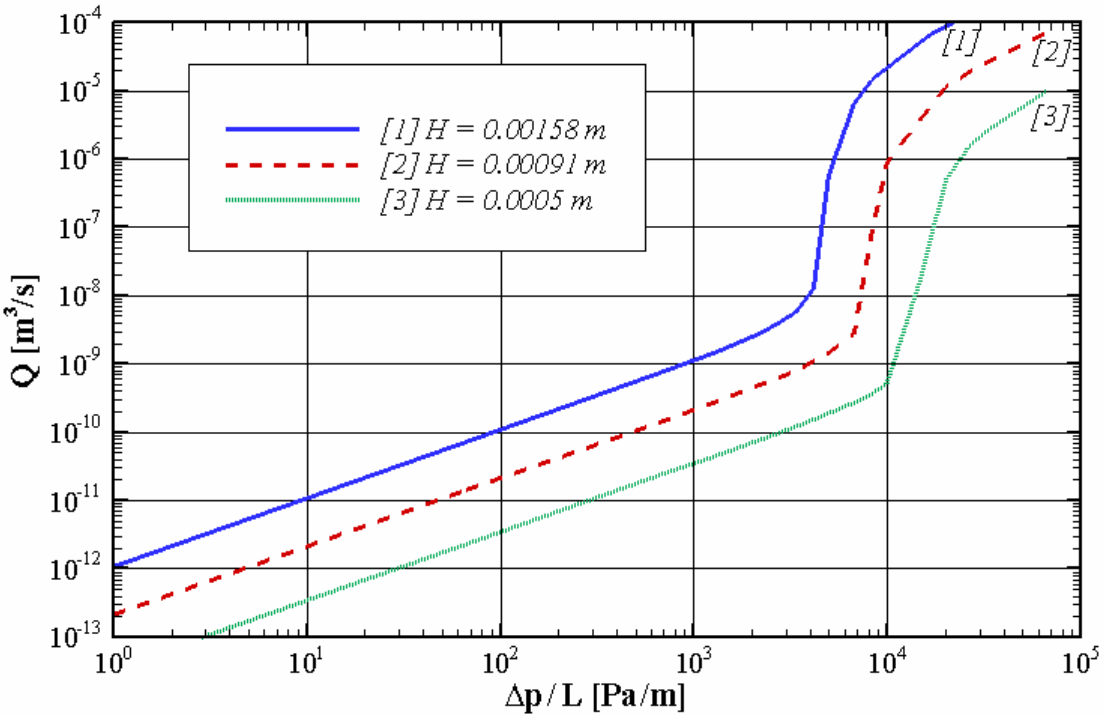

SF6 - Height variation

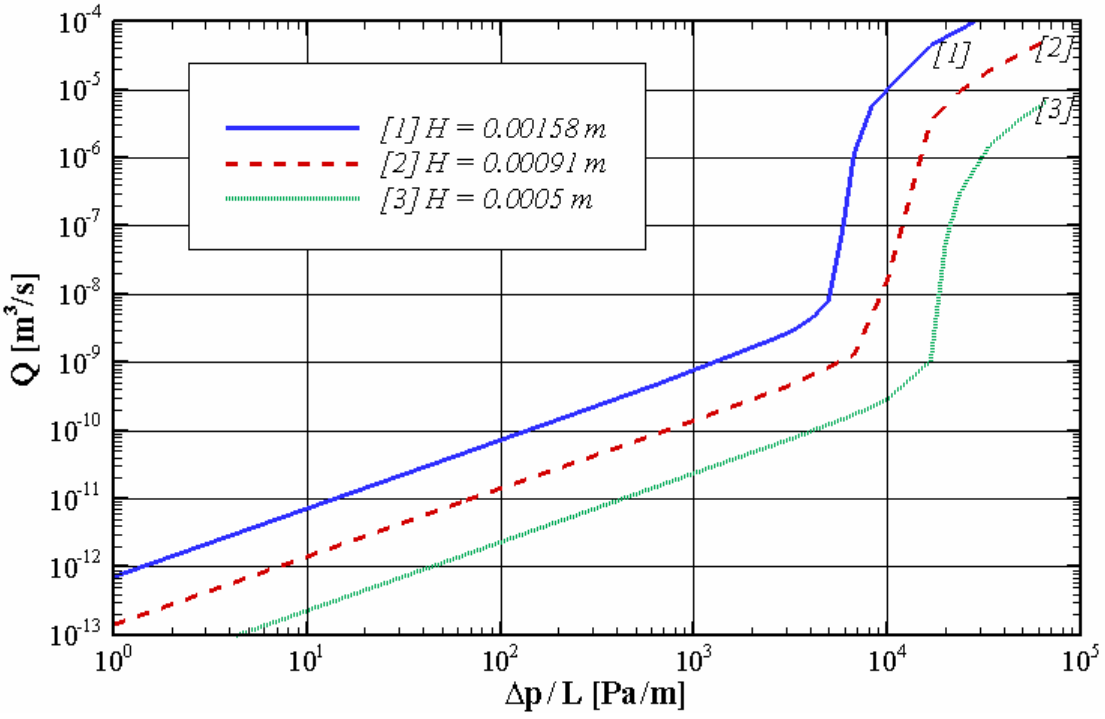

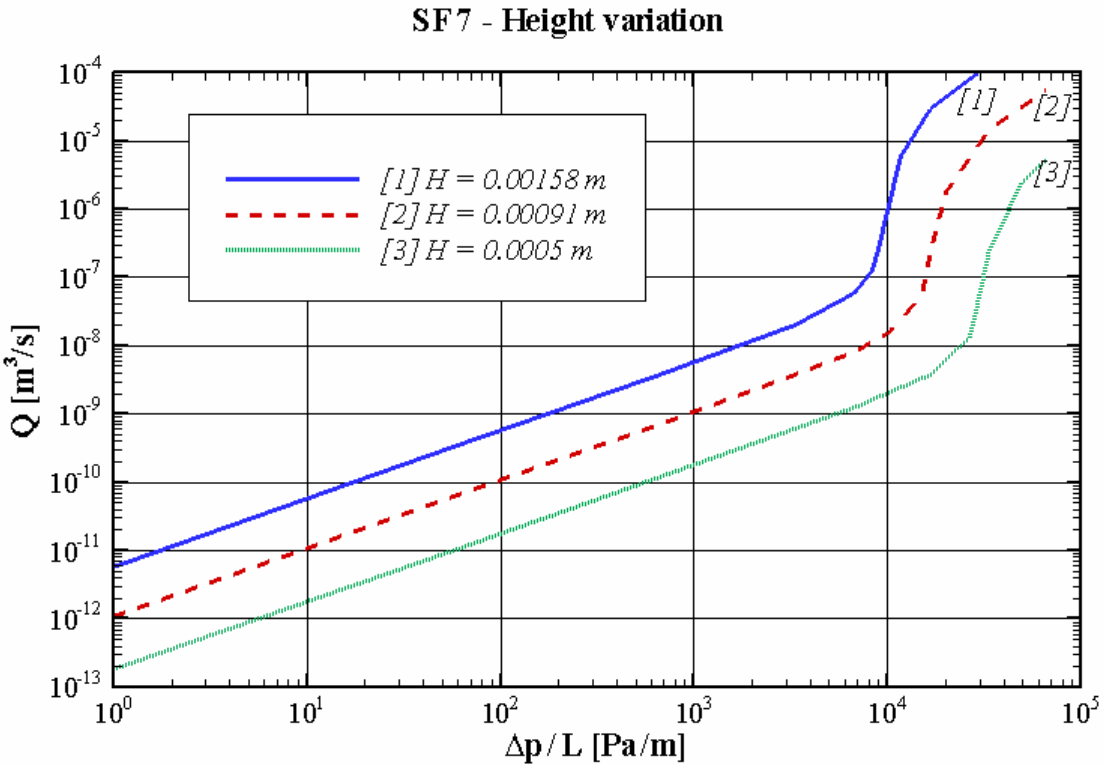
SF 7 - Height variation
[1] H = 0.00158 m
[2] H = 0.00091 m
[3] H = 0.0005 m
[1]
[2]
[3]
Q [m³/s]
Δp / L [Pa/m]

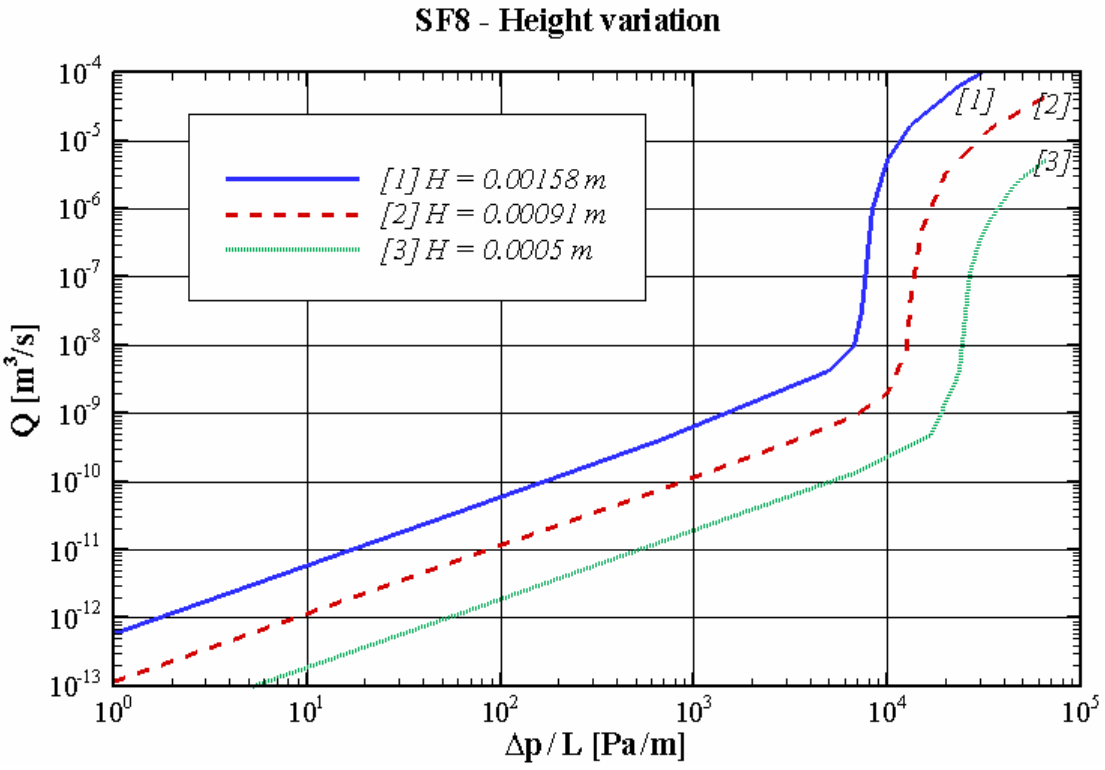
SF8 - Height variation
[1] H = 0.00158 m
[2] H = 0.00091 m
[3] H = 0.0005 m
[1]
[2]
[3]
Q [m³/s]
Δp / L [Pa/m]

SF9 - Height variation

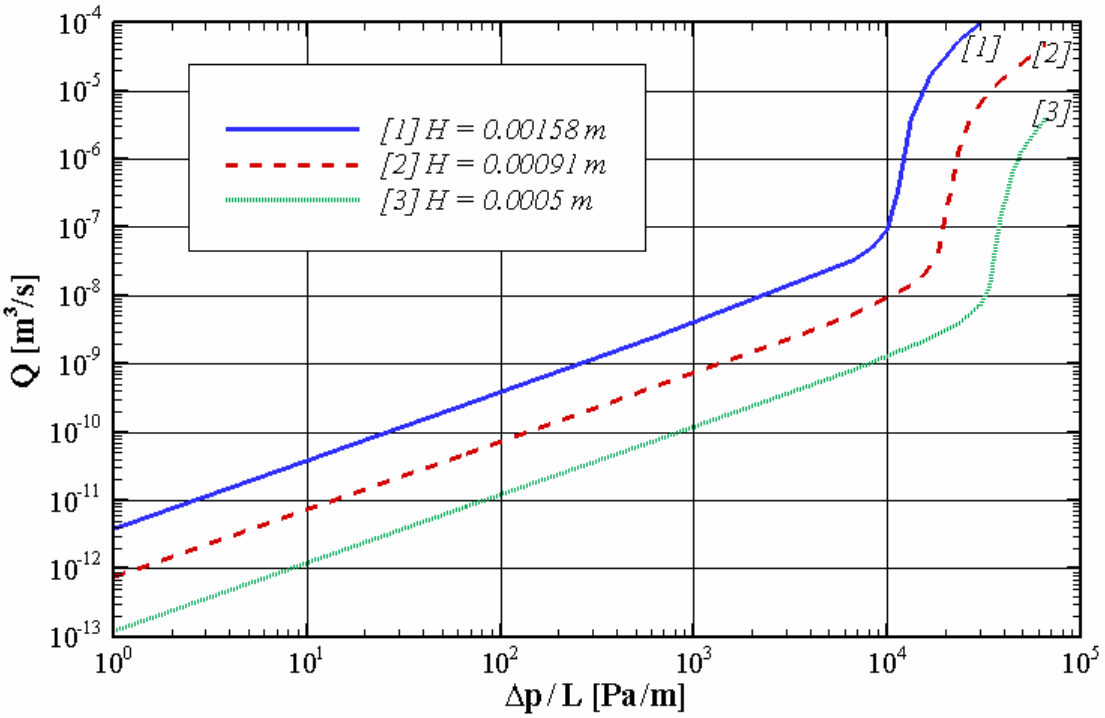

SF10 - Height variation